Journal of Molecular Liquids xxx (xxxx) xxx

Contents lists available at ScienceDirect

Journal of Molecular Liquids

journal homepage: www.elsevier.com/locate/molliq

Self-assembly of quasicrystals and their approximants in fluids with bounded repulsive core and competing interactions

Gianpietro Malescio [a,*], Francesco Sciortino [b]

[a] Dipartimento di Scienze Matematiche e Informatiche, Scienze Fisiche e Scienze della Terra (MIFT), Università di Messina, Viale F. Stagno d'Alcontres, 31, I - 98166 Messina, Italy
[b] Dipartimento di Fisica, Università di Roma "La Sapienza", Piazzale A. Moro 5, I – 00185 Roma, Italy

ARTICLE INFO

Article history:
Received 17 August 2021
Revised 17 October 2021
Accepted 23 November 2021
Available online xxxx

Keywords:
Self-assembly in complex liquids
Quasicrystals
Cluster formation
Soft matter
Fluids with microscopic competing interactions
Fluids with bounded repulsive core

ABSTRACT

We study through numerical simulations the phase behavior of a 2D system of particles interacting through a Gaussian repulsive core supplemented with a short-range attraction and a long-range repulsion. We find that the system investigated forms a variety of crystals, a phase characterized by stripe patterns, and quasicrystalline phases displaying 8-fold, 12-fold, and 18-fold symmetry. We discover that, in a narrow density range, particles self-assemble into remarkable clusters with dodecagonal symmetry, a phenomenon to our knowledge never reported previously in the literature.

1. Introduction

Self-assembly is the process in which a disordered system of pre-existing components, be it molecules, polymers, colloids, or macroscopic particles, spontaneously forms organized structures as a result of interactions among the components, without external driving. Quasicrystals (QCs) - a growing group of materials characterized by non-periodic order - are a peculiar class of self-assembled structures. A quasicrystalline pattern can continuously fill all available space, but it lacks translational periodicity. The aperiodicity is revealed in the unusual symmetry of the diffraction pattern, which displays crystallographic forbidden rotational symmetries (e.g. 5-fold, 8-fold, 10-fold, 12-fold, 18-fold). Often, in the same system, quasicrystals coexist with their approximants, i.e. ordinary crystals that are built from the same structural subunits of quasicrystals, but arranged in a periodic way, representing the link between quasicrystals and periodic crystals.

Since the first observation of a decagonal quasicrystal in Al–Mn alloys [1], many metallic QCs have been discovered [2]. Subsequently QCs have been observed in an increasingly number of soft-matter systems [3–7]. Compared with metallic QCs, soft materials are more promising candidates for self-assembling mono-component QCs. Moreover, in comparison with atomistic quasicrystals, colloidal quasicrystals are orders of magnitude larger. Due to the complex non-periodic structures on nano- to micrometer length scales, colloidal quasicrystals are natural candidates for advanced photonic materials in a range of optical devices [8,9]. Self-assembled soft-matter quasicrystals are thus of interest for a number of reasons, not least because they promise to provide a route to manufacturing materials and coatings with novel optical or electronic properties arising as a consequence of their high degree of rotation symmetry [10,11].

Since in soft materials the interaction between particles can be tuned in various ways, soft systems are also well suited for investigating how self-assembly depends on the interaction features. This has stimulated the interest in understanding the mechanisms by which soft-matter QCs can form. Formation of quasicrystals was reported (in numerical studies) for several mono-component systems with a variety of interactions: these include isotropic potentials with competing length scales [12–15] and anisotropic particles naturally possessing multiple length scales, such as patchy particles [16] and spherical building blocks functionalized with mobile surface entities [17]. In most studies, particles interact via an infinitely repulsive core decorated with additional components. Only few authors [18,19] considered systems of soft core particles interacting through potentials that are finite at the origin, a feature that, though being non-physical for atomic systems, is relevant in the realm of soft matter, where effective interactions among soft,

* Corresponding author.
E-mail address: malescio@unime.it (G. Malescio).

https://doi.org/10.1016/j.molliq.2021.118209
0167-7322/

flexible macromolecules such as polymer chains [20], dendrimers [21], polyelectrolytes, etc. may result in a bounded short-range repulsion. A typical example is the well-known GCM (Gaussian core model) [22], a model able to describe in an excellent approximation the repulsive entropic interactions between the centers of mass of two polymer chains.

We here study the phase behavior of a 2D system of particles interacting through a Gaussian repulsive core supplemented by a short-range attraction and a long-range repulsion. This system has been considered in a previous study where the formation of aggregates of particles was investigated [23]. We find, through molecular dynamics simulations, that the investigated system forms a variety of crystals, a phase displaying stripe patterns, and a number of quasicrystals characterized by 8-fold, 12-fold, and 18-fold symmetry. At high densities, crystals are characterized by the presence of sites with multiple occupation, a phenomenon which is allowed by the finite nature of the repulsion at the origin. In a narrow density range the system is characterized by the formation of remarkable clusters having full dodecagonal symmetry, a feature to our knowledge never reported previously in the literature.

2. Model

We consider a 2D system of particles interacting through the following potential:

$$\frac{U(r)}{\varepsilon} = \exp(-(r/R)^2) - w \cdot \exp[-((r/R)-2)^2] + \alpha \cdot \exp[-((r/R)-3)^2] \cdot f(r) \quad (1)$$

where r is the interparticle distance, ε and R are arbitrary energy and length units, respectively, w and α are the strength of the short-range attraction and of the long-range repulsion, respectively, and $f(r)$ is the function:

$$f(r) = \frac{1}{1+\exp\left[\frac{3-(r/R)}{0.1}\right]} \quad (2)$$

Throughout our investigation ϵ is the unit of energy (and temperature, choosing Boltzmann constant $k_B = 1$) and R is the unit of length. With this choice, $\epsilon = 1$, $R = 1$. Moreover, we choose $w = 0.05$. The potential $U(r)$ defined in Eq. (1) is composed of three terms: a finite repulsive core having the form of a gaussian centered at the origin, an attractive component consisting in a negative gaussian centered at $r = 2$ having fixed strength w, and a repulsive long-range term which is given by the product of a gaussian centered at $r = 3$ times the function $f(r)$, which is a continuous function approximating a Heaviside step function that goes from 0 to 1 around $r = 3$. This specific form of the long-range repulsion makes it possible to vary its strength, i.e. α, without significantly affecting the inner repulsion and attraction. The potential $U(r)$ is shown in Fig. 1 for $\alpha = 0.05$. With this choice of parameters, the potential has a minimum at $r_{min} = 2.27$, with $U(r_{min}) = -0.04$ and a secondary maximum at $r_{max} = 3.36$, with $U(r_{max}) = 0.035$.

3. Methods

We have investigated the properties of a system of particles interacting through the potential described in Eq. (1) via Molecular Dynamics (MD) simulations. MD simulations have been performed with standard home-written codes in the NVT and NPT ensembles. In the NVT ensemble, the velocity Verlet algorithm has been used to integrate the equation of motion, supplemented by the Andersen thermostat. In the NPT ensemble, we have selected a mixed

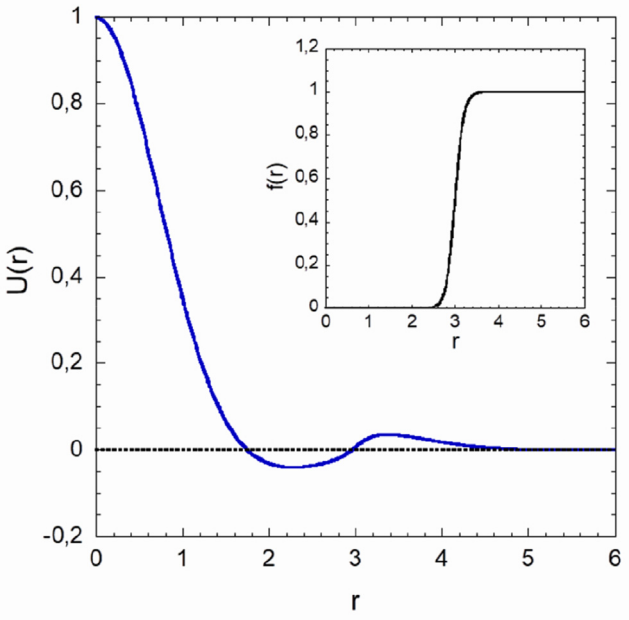

Fig. 1. Interaction potential U(r) defined in Eq. (1); $\alpha = 0.05$. The function f(r) is shown in the inset.

MD-MC scheme, where a Monte Carlo move in which each of the box lengths (along x and y) is varied by a random quantity (and accepted with the proper MC acceptance rule [24]), is randomly alternated with a 200 steps NVT MD simulation. We have verified that the pressure imposed in the MC part coincides with the average pressure measured with the standard virial expression.

We have studied systems of N = 1000 particles (though in some investigations we used N = 16000 and N = 25000) in two dimensions. As usual, time is expressed in units of $\sqrt{mR^2/\epsilon}$ where $m = 1$ is the mass of the particle. In these units, the timestep is 0.01. Pressure is measured in units of ϵ/R^2. We study the system at a temperature $T = 0.01$ in a wide range of values of the surface density ρ (measured in units of $1/R^2$).

4. Results

4.1. Gas phase

We first considered small densities ($\rho < 0.10$), where the system is in the gas phase. In a previous investigation [23], we found that a three-dimensional system of particles interacting through the potential here considered, at low densities is characterized by the presence of polydisperse clusters. In order to analyze the possible aggregation of particles with the resulting formation of clusters in the 2D system, we calculated the probability distribution $P(s)$ of finding clusters of size s for several densities. Particles are considered as bonded if their distance is smaller than the position of the maximum r_{max} of the long-range repulsive component of the interaction ($r_{max} = 3.36$). Particles are assumed to be part of the same cluster if there is a continuous path of bonds connecting them.

As shown in Fig. 2, the cluster size distribution $P(s)$ becomes wider and wider on increasing the density ρ, so that a spanning cluster (indicative of a percolation transition) eventually develops around $\rho \sim 0.10$. The distribution $P(s)$ shows a weak peak, indicating a preferred cluster size, around $s \approx 3$–4.

The clustering process is manifested in the behavior of the structure factor $S(q)$ at small q (Fig. 3). Assuming that clusters

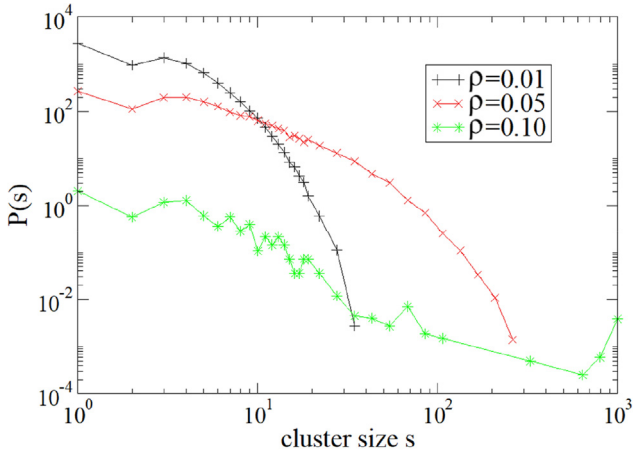

Fig. 2. Cluster size distribution $P(s)$ vs. cluster size s at T = 0.01, for several densities (number of particles N = 25000). $P(s)$ is normalized such that $\Sigma\, sP(s) = N$.

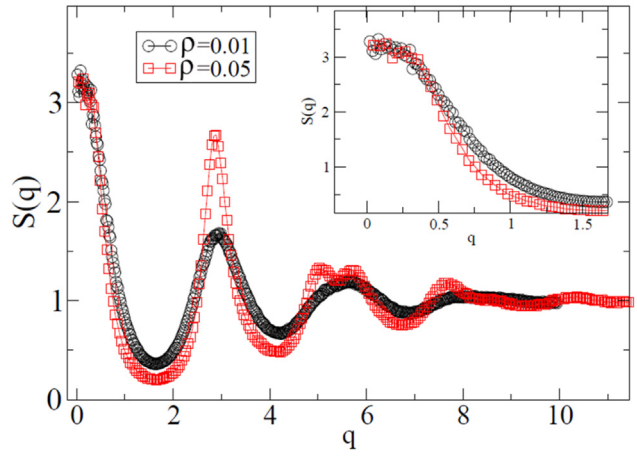

Fig. 3. Structure factor calculated at a temperature T = 0.01 for ρ = 0.01, 0.05 (number of particles N = 1000). The inset shows $S(q)$ for a system of N = 25000 particles, to highlight the small q behavior.

are uncorrelated in space, the system can be considered as an ideal gas of clusters, so we can use the ideal gas formulas for pressure and compressibility.

More precisely,

$$P = k_B T N_{cluster}/A, \quad \chi_T = 1/(k_B T N_{cluster}/A)$$

where $N_{cluster}$ is the total number of clusters in the system of surface A.

From the well-known long-wavelength limit of the structure factor

$$S(q=0) = \rho k_B T \chi_T$$

it follows that

$$S(q=0) = N/N_{cluster}$$

Since N is approximately equal to $N_{cluster}$ times the average cluster size $\bar{s}$, the limit of $S(q)$ for q approaching zero is set by $\bar{s}$.

The ideal gas of cluster hypothesis can be checked independently both by counting the number of clusters and predicting the pressure (and the compressibility) as well as calculating the average cluster size $N/N_{cluster}$. Both checks are satisfied by the data.

4.2. Crystalline and quasi-crystalline phases

The system considered exists as a gas phase only at very low pressures (smaller than 0.005). At higher pressures it shows a very rich scenario of crystalline and quasi-crystalline phases. In order to calculate the equation of state $P(\rho)$, we performed NPT MD simulation at several pressures in the range $0.00001 \leq P \leq 1.5$.

To facilitate the identification of the numerous phases, the equation of state is shown in Fig. 4 in three different pressure intervals. The occurrence of phase transitions is indicated through the red arrows (arrows point at phases with approximately equal pressure and different densities). In the regions between two successive phase transitions, the points laying on the line representing $P(\rho)$ belong to the same phase.

We report below, for several significant (ρ,P) state points, a snapshot of the particle configuration as obtained at the end of a MD-NPT run of the order of $\sim 5{\cdot}10^8$ integration timesteps. Each particle is represented as a circle having radius r = 0.2. For each snapshot we show also the corresponding bidimensional structure factor in the plane q_x, q_y. Next, we discuss the different phases observed.

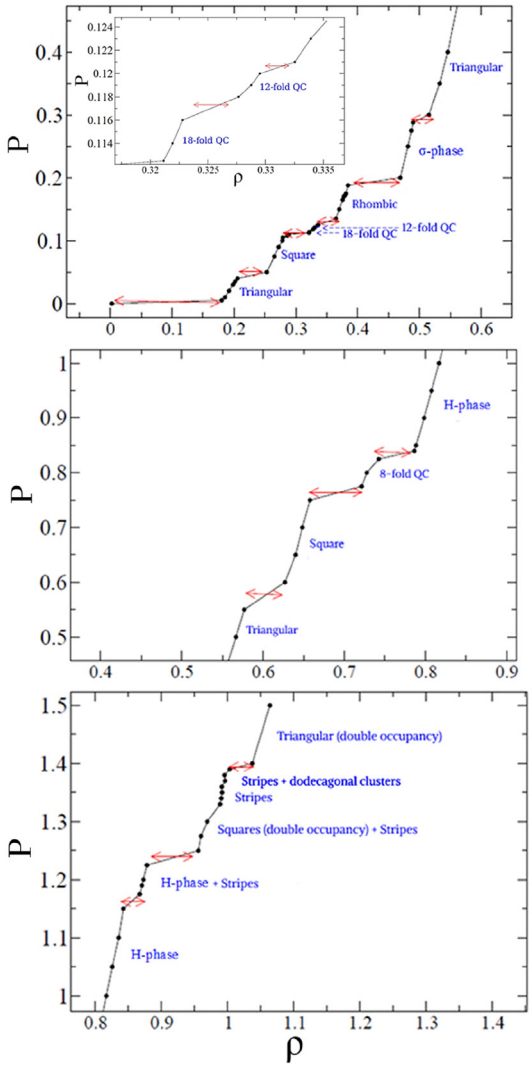

Fig. 4. Equation of state $P(\rho)$ (MD-NPT simulation). T = 0.01 (number of particles N = 1000). Red arrows indicate first order phase transitions. The blue labels specify the different phases.

Upon increasing pressure (starting from the gas phase), the system crystallizes at first in a triangular phase (e.g. at P = 0.04), and then in a square phase (e.g. at P = 0.09). This behavior is the opposite of what happens for systems with infinitely repulsive core, such as, e.g., hard disks, where the triangular lattice is preferred at high densities, since it is more efficient at filling the plane with respect to the square lattice. In fact, the densest packing of hard disks in the plane is attained by arranging them in the triangular-hexagonal lattice, with maximum packing fraction $\eta_{max} \approx 0.9069$, whereas a square lattice attains $\eta_{max} \approx 0.7854$ (in 2D systems the packing fraction is $\eta = \frac{\pi}{4}\rho d^2$, where ρ is the number density and d is the hard disk diameter). The reason for the "inversion" observed in the system investigated is related to the soft nature of the repulsion. Since as the density increases, repulsion loses its efficacy, in certain density ranges increasing the number density results in making available additional space to the particles, as a consequence of the decreasing effective particle radius. Thus, the decreased efficacy of the long-range repulsion makes it possible for the system to crystallize in a less efficient space-filling lattice, in spite of the increased density.

Upon further increasing the pressure, in a restricted range of pressures ($0.112 < P < 0.121$) the system displays two quasicrystalline phases characterized by non-periodic order. More precisely, the system forms an 18-fold symmetric quasicrystal in the pressure interval $0.1125 \leq P \leq 0.116$, and a 12-fold symmetric quasicrystal in the pressure interval $0.118 \leq P \leq 0.12$ (see inset in the top panel of Fig. 4).

Fig. 5 shows the particle configuration and the corresponding structure factor at P = 0.114 . In order to make evident the local arrangement of the particles, in a few portions of the snapshot we connected neighbouring particles through segments. In addition to tilings such as pentagons, flattened hexagons and quadrangles, we observe the presence of nonagons (with a central particle), that are generally surrounded by pentagons. The structure factor exhibits an evident 18-fold symmetry, a crystallographic forbidden rotational symmetry, characteristic of an octadecagonal quasicrystal. We show also a 3d representation of the structure factor, where the lowest values of $S(q)$ have been cut off and the bases of the highest peaks have been connected so to highlight the two inner shells in the reciprocal space. Analogous features, both as it regards the particle configuration and the structure factor, were observed at $P = 0.1125, 0.116$.

In the pressure range $0.118 \leq P \leq 0.12$ the structure factor is characterized by the presence of 12 peaks in the inner shell in the reciprocal space (Fig. 6). This feature is an indication of a 12-fold rotational symmetry. However, only the peaks in the first shell are well defined, while those of the second shell are rather broad, which suggests that a certain amount of disorder is present in the quasicrystalline arrangement. Indeed, though in the snapshot one can observe the presence of tilings (not highlighted in the figure) such as pentagons, flattened hexagons, few quadrangles, and a couple of nonagons, these tilings are in general rather loosely defined.

As pressure increases, the system crystallizes first into a rhombic phase, in a range of pressures around P = 0.15, and then, in the pressure range $0.2 \leq P \leq 0.3$, we observe a phase with particles

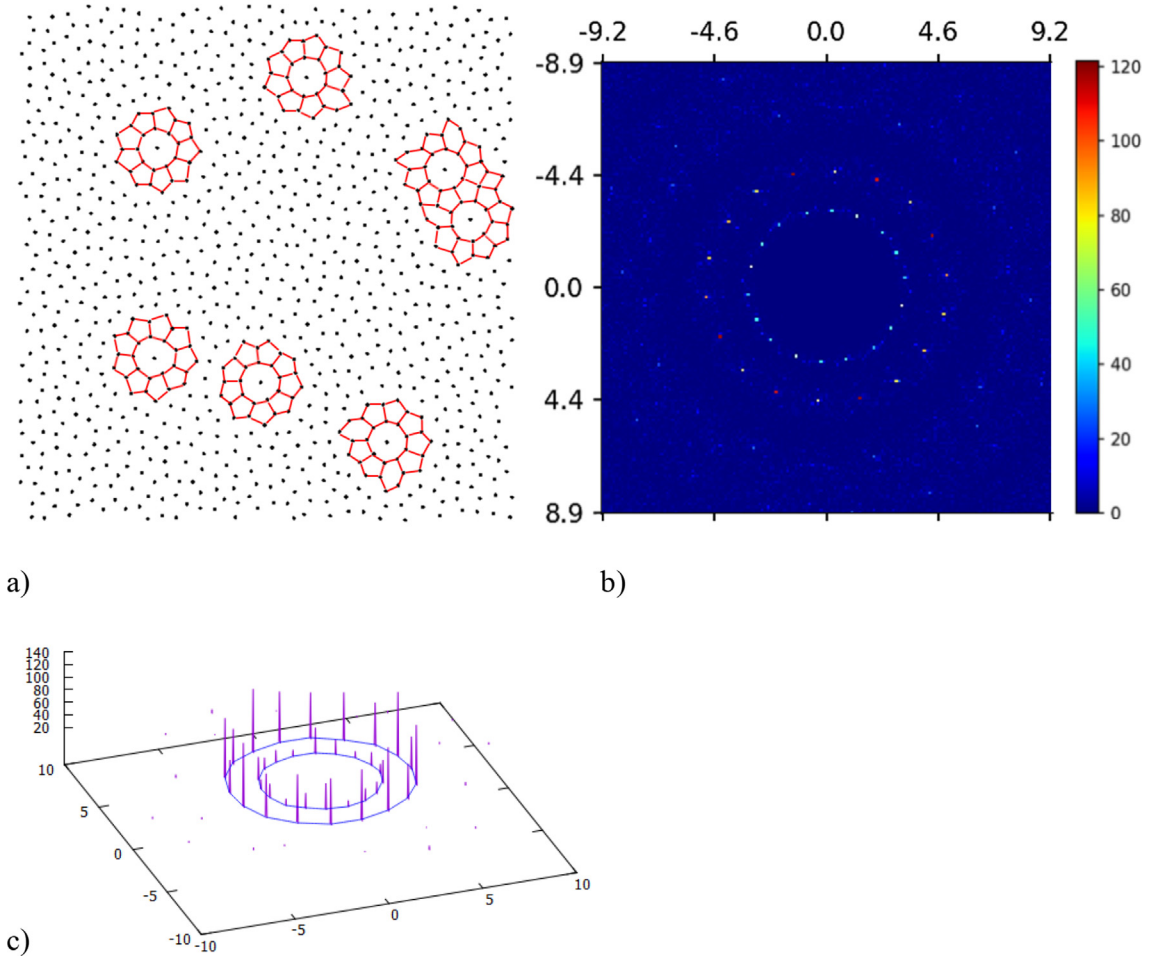

Fig. 5. 18-fold QC phase (ρ = 0.3217 ± 0.0005, P = 0.114). (a) Particle configuration; b) diffraction pattern (map view); c) 3d representation of the diffraction pattern.

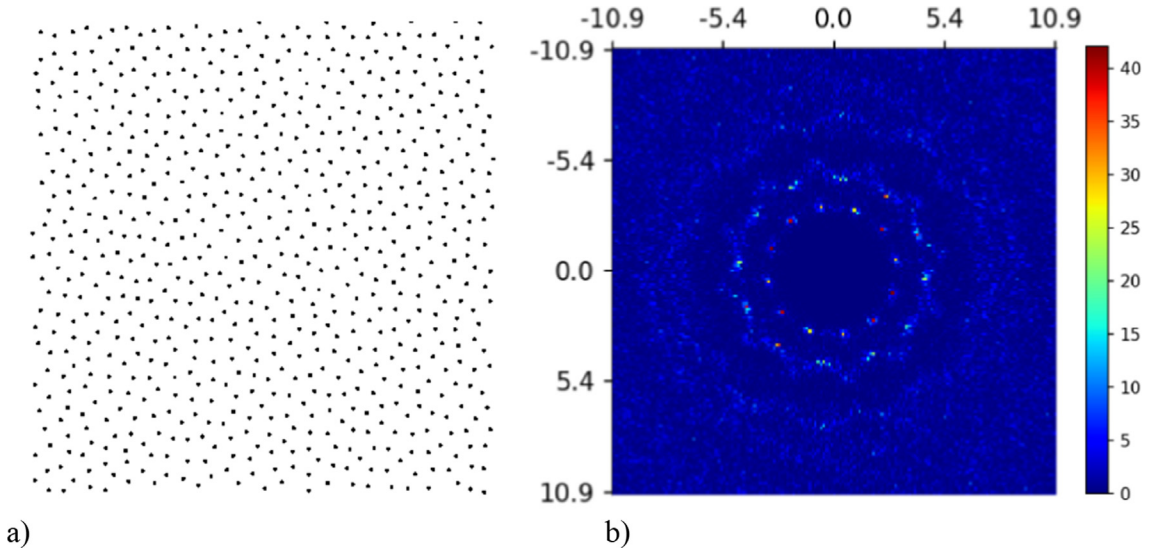

Fig. 6. 12-fold QC ($\rho = 0.328 \pm 0.0005$, P = 0.119). a) Particle configuration; b) diffraction pattern.

arranged on squares and triangles (Fig. 7). In a square-triangle tiling, each particle is simultaneously the vertex of two squares (2x90°) and three equilateral triangles (3x60°), for a total of 360°. Depending on the local arrangement of squares and triangles around the central particle, environments can be categorized as σ-type (where contiguous squares have in common only one vertex) or H-type (where contiguous squares share one side) in analogy to the Frank-Kasper phases [25–26] (see the insets of Fig. 7 and Fig. 9). Both these phases are considered as crystalline approximants to dodecagonal quasicrystals. We connected particles in a portion of Fig. 7 so to make evident that the crystalline structure is typical of a σ-phase.

For $0.3 \leq P \leq 0.55$, the system crystallizes in a triangular lattice, whereas for $0.6 \leq P \leq 0.75$ the crystal displays a square lattice. Thus, similarly to what observed for $P \leq 0.1$, with increasing pressure, the decreasing efficacy of the soft repulsion (now tested at inner distances) makes available additional space to the particles, which allows the system to crystallize in the less efficient space-filling square lattice, in spite of the higher density.

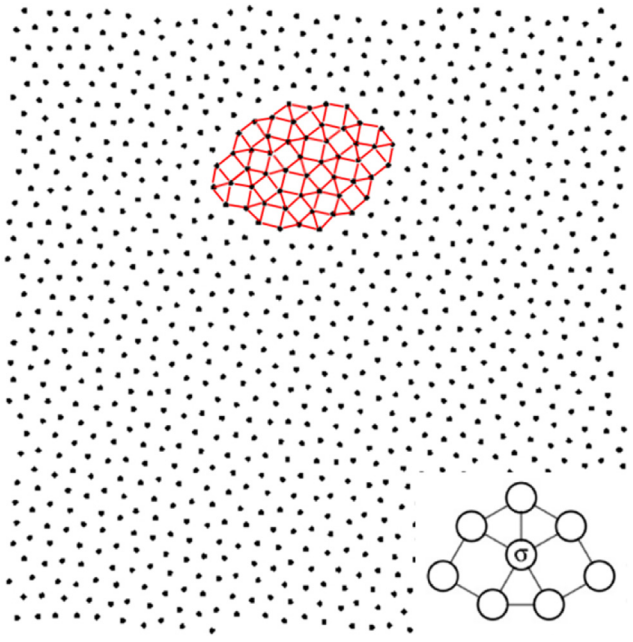

Fig. 7. σ-phase ($\rho = 0.4812 \pm 0.0005$, P = 0.25). Particle configuration; inset: σ-type local environment.

In the pressure range $0.755 \leq P \leq 0.825$, we observe a phase whose structure factor shows an 8-fold symmetry typical of an octagonal quasicrystal (Fig. 8). By connecting particles in portions of the snapshot we make evident that particles are arranged mainly on octagons (with a central particle) and pentagons. Octagonal rings may be directly in contact or separated by pentagonal tiles surrounding the ring. The diffraction pattern shows an octagonal symmetry, with peaks arranged in concentric octagons, as is evident both from the map view and the 3d representation.

In the pressure range $0.84 \leq P \leq 1.15$, particles are arranged according to a tiling that closely resembles one of the Archimedean lattices, the $(3^2,4^2)$ tiling, also called trellis tiling, with each vertex of the tiling occupied by a single particle (Fig. 9). With respect to the trellis tiling, which is made up of squares and equilateral triangles, the tiling pattern in the configuration shown here is slightly elongated along the direction coincident with the axis of the columns of squares. Aside from this distortion, the local environment is of the H-type.

For $P > 1.15$, particles begin to overlap with each other. In spite of being finite at the origin, and thus allowing particle superposition, the Gaussian repulsion does not favor particle overlapping since this has nevertheless an energetic cost. However, when an extra particle is inserted in a dense enough configuration of particles, the partial overlap of its long-range repulsion with the repulsive tails of the numerous neighboring particles would imply a higher energetic cost with respect to the complete overlap of the extra particle with just one of the pre-existing particles. Particle overlaps are thus energetically preferred as the density increases.

As the pressure increases, dimers (i.e. couples of particles with interparticle distance $r < 0.3$) organize so to form worm-like stripes alternated with parallel stripes of single particles. Around $P = 1.2$, the system shows a mixed phase displaying regions characterized by the trellis tiling and regions with alternating stripes of dimers and single particles. At $P = 1.35$, the stripe pattern extends over the whole system. To make evident the spatial distribution of the overlaps, we represent dimers as red dots, and single particles as black dots (Fig. 10). It can be observed that within "black" stripes the distance between adjacent particles is approximately half than

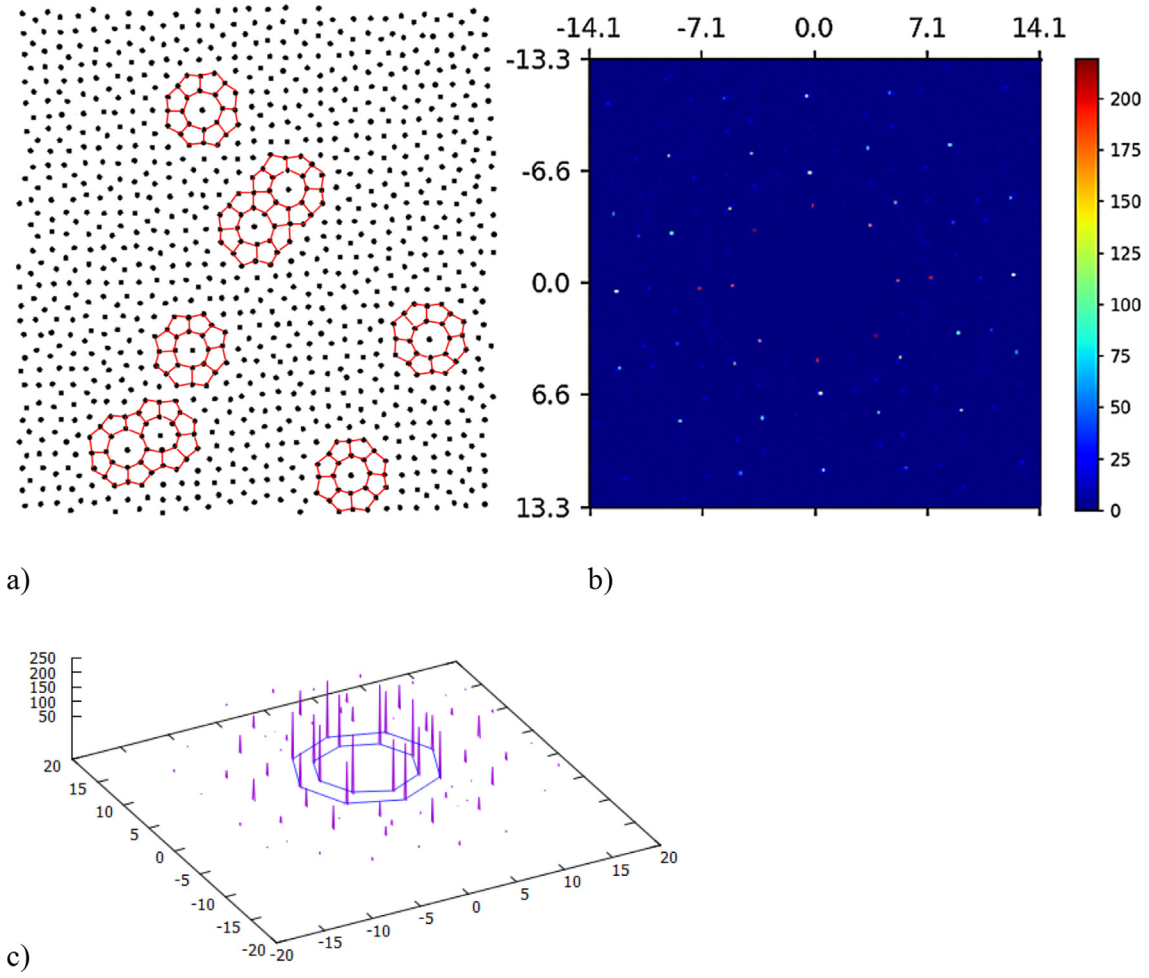

Fig. 8. 8-fold QC ($\rho = 0.743 \pm 0.0005$, P = 0.825). a) Particle configuration; b) diffraction pattern (map view); c) 3d representation of the diffraction pattern.

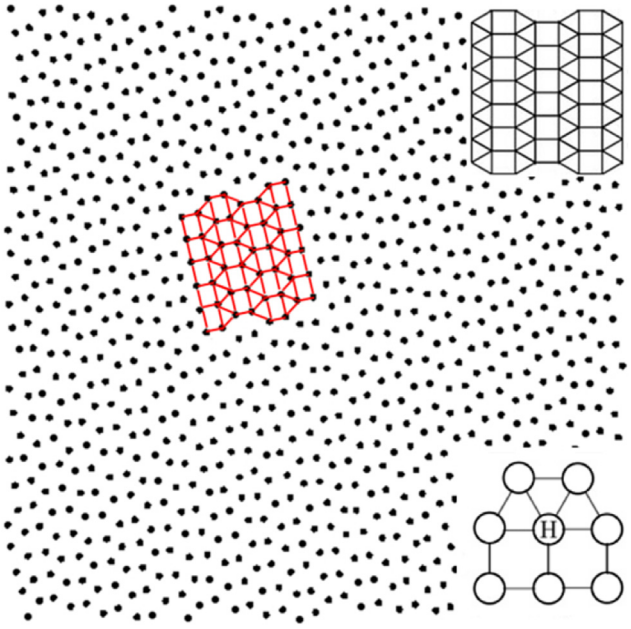

Fig. 9. H-phase ($\rho = 0.8058 \pm 0.0007$, P = 0.95). Particle configuration. Upper inset: trellis Archimedean tiling; lower inset: H-type local environment.

the distance between adjacent dimers in "red" stripes. Thus, the overall number of particles per unit length along the black stripes or along the red stripes is roughly the same. The points of the reciprocal lattice are arranged according to the $(2^2,8^2)$ Archimedean lattice, or CaVO tiling.

Stripe patterns analogous to those present in the snapshot in Fig. 10 can be generated starting from the H phase and proceeding as follows: for each square of the trellis tiling, leave two adjacent particles in their place and move the two on the opposite side of the square so that they overlap in the midpoint of the side, as better illustrated in Fig. 11.

Upon slightly increasing the pressure (and the density) a novel remarkable feature emerges. In addition to stripes of sites with single and double occupancy, dodecagonal clusters of particles appear. This new feature is quite evident in the particle configuration shown in Fig. 12, obtained by performing MD NVT simulations at $\rho = 1.0$. A significant number of clusters are present in the snapshot. Moreover, in a portion of the snapshot we observe a triangular lattice, where the basis added to each lattice point is a dodecagonal cluster. A triangular crystal of this type represents an approximant to a dodecagonal quasicrystal [14]. Accordingly, the structure factor $S(q)$ corresponding to the snapshot exhibits an evident 12-fold symmetry.

At such densities, particle overlapping is quite relevant, as made evident by the high number of red dots in the snapshot. Accordingly, the radial distribution function (not shown) has its highest peak at r = 0.

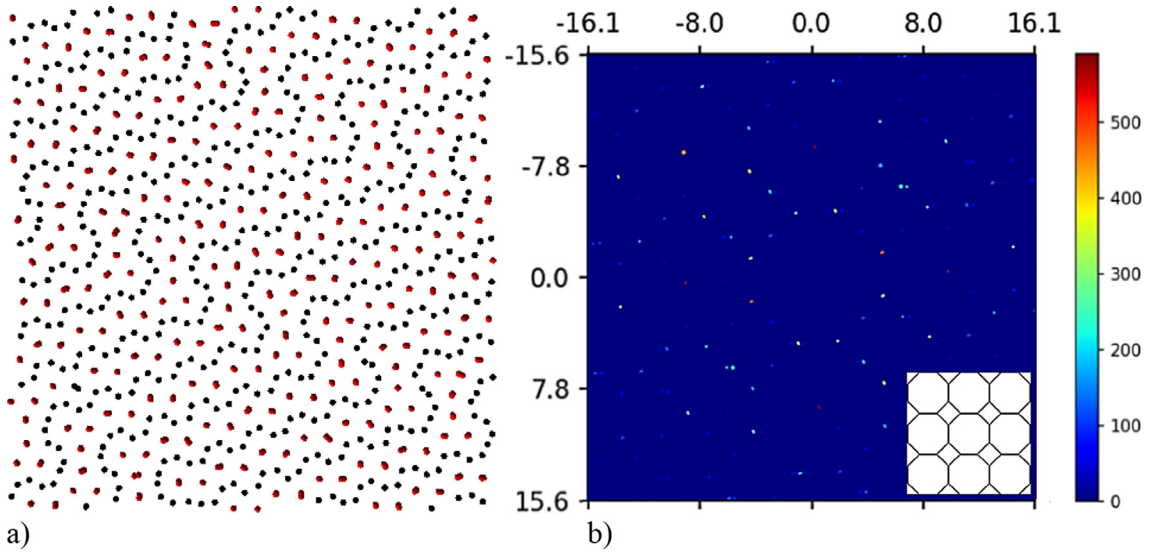

Fig. 10. Stripe phase ($\rho = 0.9915 \pm 0.001$, $P = 1.35$). a) Particle configuration. Black dots represent single particle, red dots represent dimers (i.e. two particles with interparticle distance $r < 0.3$); b) diffraction pattern; inset: CaVo Archimedean tiling.

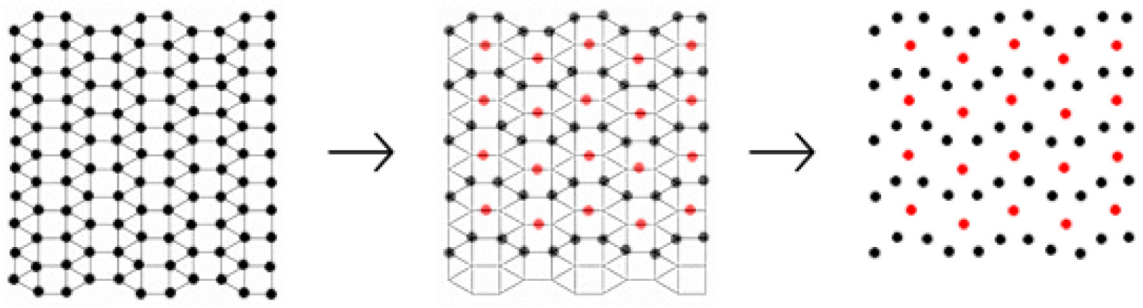

Fig. 11. From trellis tiling to alternated stripes of dimers and single particles.

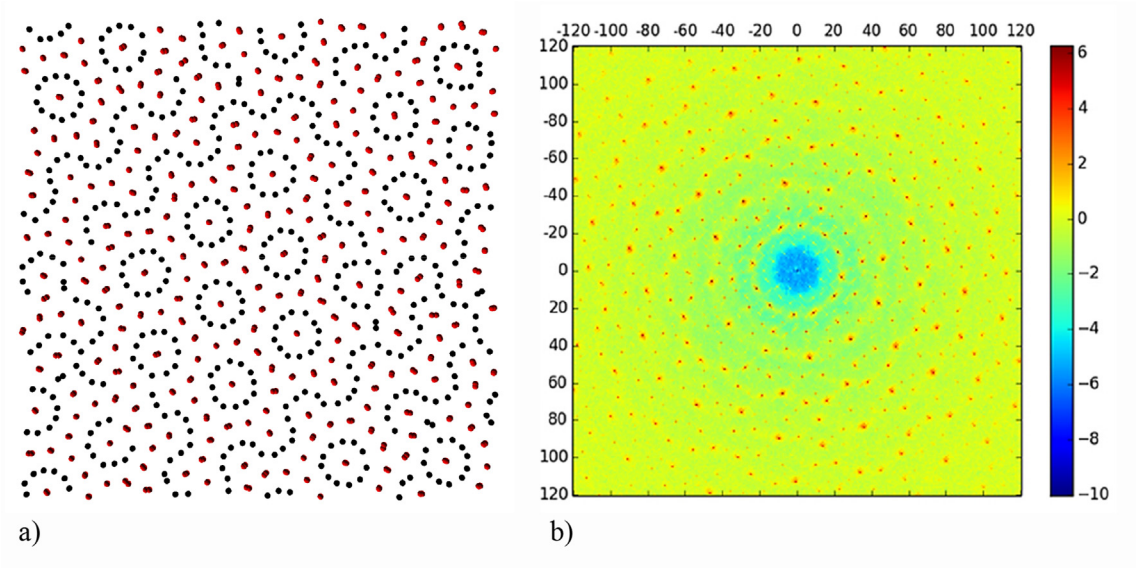

Fig. 12. MD NVT simulation. Particle configuration and corresponding structure factor at $\rho = 1.0$ (and $T = 0.01$). a) Particle configuration; b) diffraction pattern (the intensity values are here shown in a logarithmic scale).

To check the possibility that the system might crystallize into a triangular lattice, we performed very long runs, but independently of the run length only limited portions of the system display a crystalline triangular arrangement. However, when performing simulation starting from a triangular crystal of dodecagonal clusters, we found that the crystal is mechanically stable.

Let us now examine more in details the nature of the dodecagonal clusters observed. Each cluster consists in a central site surrounded by twenty-four sites arranged in two concentric circumferences. In each circumference there are twelve approximately equally-spaced sites. The radius of the external circumference is slightly smaller than twice the radius of the inner circumference (which is approximately 1.4). In a hypothetically isolated cluster, the central site of each cluster is doubly occupied, while the other sites are singly occupied (see Fig. 13). However, when clusters develop in the system, the sites of the second circumference overlap with those of adjacent clusters (thus becoming doubly occupied) as can be appreciated in Fig. 12.

The geometrical structure of each cluster consists in a 12-fold rosette of rhombs with 30° acute angles. The sites occupied by the particles in the cluster coincide with the vertices of the rhombs. This geometrical structure has been used as a starting point to build through recursive relations quasiperiodic tilings with 12-fold rotational symmetry of interest in the study of quasicrystals, such as the Socolar 12-fold A tiling, obtained by combining thin rhombs, thick rhombs, and squares, or some of Stampfli 12-fold tilings, obtained combining thin rhombs, equilateral triangles and squares, or just thin and thick rhombs [29].

Dodecagonal quasicrystals formed by real systems, as well as those obtained through simulation of model systems, are more commonly described in terms of 12-fold square-triangle tilings of particles [27]. As found in numerical simulations of systems both of isotropic particles with hard core + soft corona [14] and of non-isotropic patchy particles [16,28], a common motif formed by particles in dodecagonal quasicrystals is that shown in Fig. 13b. This motif is also frequently used to generate quasiperiodic tilings through an inflation process [27,30]. It is evident that though such motif has a dodecagonal shape, it possesses just a 6-fold symmetry.

To evaluate the presence of finite size effects we performed NVT simulations with a system of N = 16000 particles at $\rho = 1.0$ and T = 0.01. As shown in Fig. 14, the system is characterized by the presence of domains of different types: alternate stripes of particles with single and double occupancy, and regions where particles form clusters. Unfortunately, the dynamics is so slow that we were not able to follow the system till thermodynamic equilibrium is reached and the proper stable phase takes over or coexistence between two phases is reached.

Since the orientation of the different domains is essentially random, it follows that the intensity pattern in the structure factor is characterized by concentric circumferences similarly to what occurs in an isotropic system (Fig. 14, inset). However, the intensity of the peaks along each circumference is modulated in such a way that peaks are arranged in 12 equally-spaced arches of equal length.

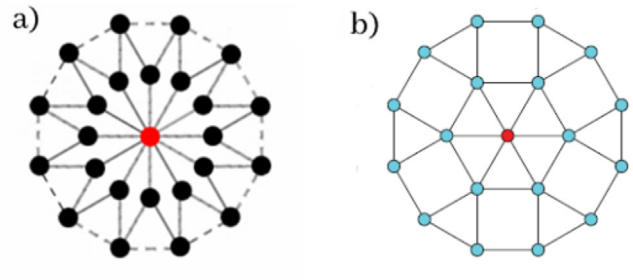

Fig. 13. a) 12-fold symmetric cluster (present paper); b) dodecagonal motif (6-fold symmetric) observed in the literature [14,16,28] (reproduced from Ref. [28]).

This is the signal of an underlying 12-fold symmetry that can be related to the regions displaying square-triangle arrangements of clusters. We consider as an example a portion of the snapshot in Fig. 14 (located close to the lower left corner of the snapshot) where clusters of particles are mainly arranged on squares and equilateral triangles. By connecting the centers of adjacent clusters, one makes evident that clusters are arranged according to a square-triangle tiling and their centers form H-type, σ-type and also hexagonal local environments (Fig. 15a). On the other hand, by connecting adjacent particles, it is possible to note that particles are arranged on thin rhombs, equilateral triangles and squares (see Fig. 15b) similarly to what occurs in the Stampfli 12-fold tiling shown in Fig. 15c.

The system investigated in the present paper, at $\rho = 1.0$ and T = 0.01 exhibits a multi-domain structure that only locally might be considered as an approximant to a dodecagonal quasi-crystal. However, at best of our knowledge, it is the only physical system, be it a real material or a model system, where particles aggregate to form dodecagonal clusters having a 12-fold symmetry, quite similarly to the motif present in the Stampfli 12-fold tiling shown in Fig. 15c. We performed also NPT calculations with N = 16000 at P = 1.36 and T = 0.01, and we obtained analogous results to those obtained through NVT simulation at ρ = 1.0, T = 0.01.

Upon further increasing the density, almost all particles overlap two by two, so the system is formed almost entirely by dimers. These are arranged at first in a triangular lattice ($\rho = 1.075$, Fig. 16a), and at higher density ($\rho = 1.2$, Fig. 16b), in a square lattice. This inversion between square and triangular lattices of dimers is analogous to that observed at lower pressures for square and triangular lattices of single particles. With increasing density or pressure, the decreasing efficacy of the soft short-range repulsion makes available additional space to the particles, so the system is allowed to crystallize in the less efficient space-filling square lattice, in spite of the increased density. As density further increases, trimers (formed by the overlapping of three particles) appear, and at $\rho = 1.7$ (Fig. 16c) we observe a square crystal of trimers and dimers. Eventually, at the highest density considered ($\rho = 2$, Fig. 16d), tetramers formed by the overlap of four particles coexist in a square lattice with trimers and few dimers.

At such high densities the behavior of the system investigated has some similarities with that of the PSM (penetrable sphere model). In fact, the PSM (in 3d) crystallizes into a fcc solid where, with increasing density (and temperature), sites are occupied by an increasing number of particles [31]. Thus, the PSM forms multiple fcc solids differing for the fractions of sites occupied by pairs, triplets, etc. As already observed in a previous paper by us [23], the presence of the interaction components (i.e. the short-range attraction and the long-range repulsion) added, in the model here considered, to the Gaussian repulsive core, modifies the re-entrant melting behavior that is typical of the Gaussian core when alone, and determines a tendency to form at high densities a clustered solid similarly to systems such as the penetrable sphere model and the GCM-4 system (which can be considered the continuous analogous of the PSM [32]). As it occurs in the PSM, we observe that at high densities a practically constant effective density of clusters is maintained in the crystal, which leads to a density-independent lattice constant. Indeed, for the three configurations shown in Fig. 16b, c, d, the radial distribution function is similar, the only difference being the height of the peak at r = 0, which increases with the density (Fig. 17).

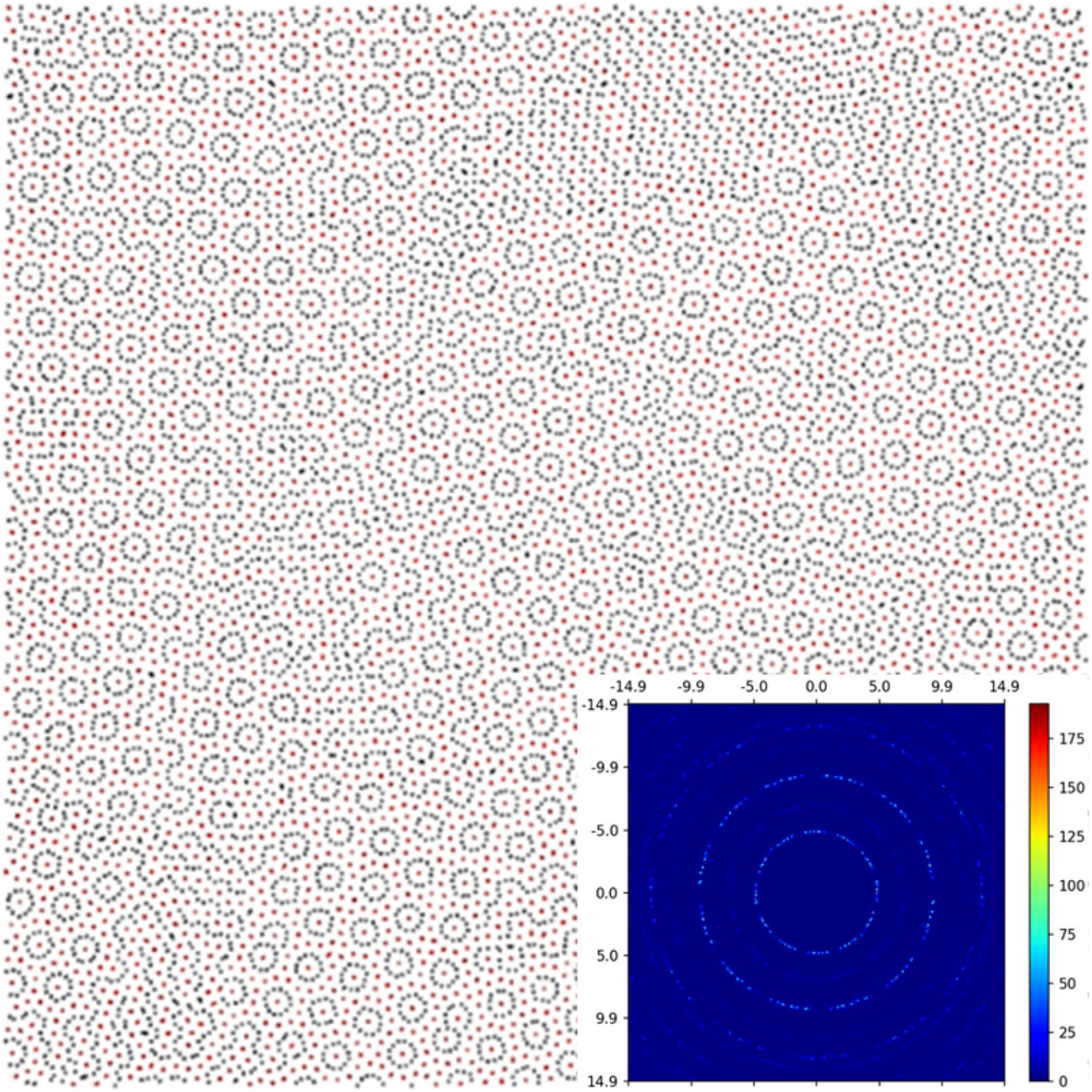

Fig. 14. ρ = 1.0, T = 0.01, N = 16000 particles. Particle configuration; inset: diffraction pattern.

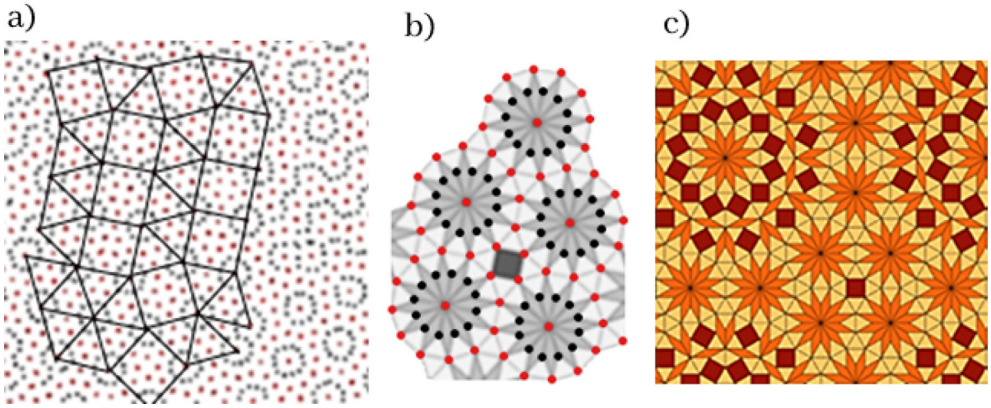

Fig. 15. a) Magnification of a region located close to the lower left of Fig. 14; b) magnification of a region located close to the upper left corner of Fig. 15a (adjacent particles are connected by lines to emphasize the cluster geometry); c) Stampfli 12-fold tiling with thin rhombs, equilateral triangles and squares (reproduced from Ref. [29]).

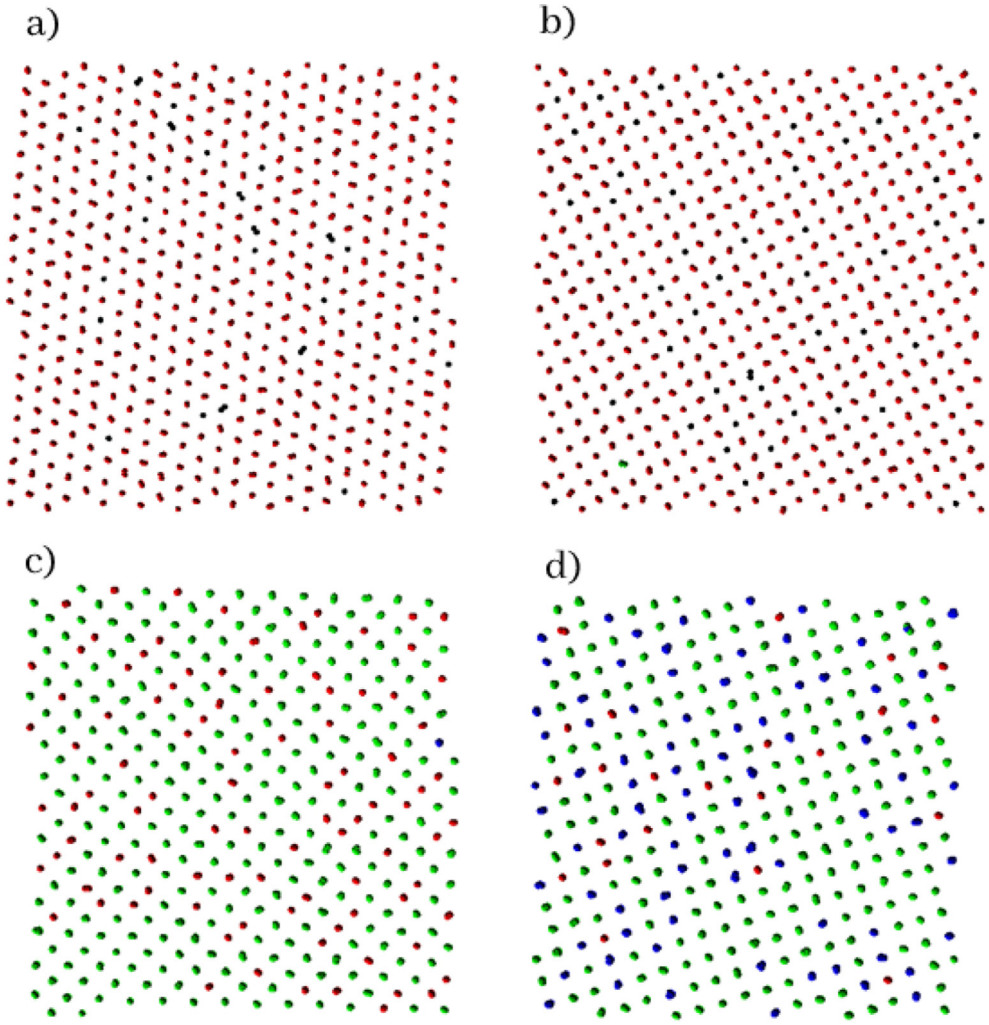

Fig. 16. Snapshots of the systems at T = 0.01 and several densities. a) ρ = 1.075. Triangular crystal of dimers; b) ρ = 1.2. Square crystal of dimers; c) ρ = 1.7. Square crystal of dimers + trimers (green dots); d) ρ = 2.0. Square crystal of dimers + trimers + tetramers (blue dots).

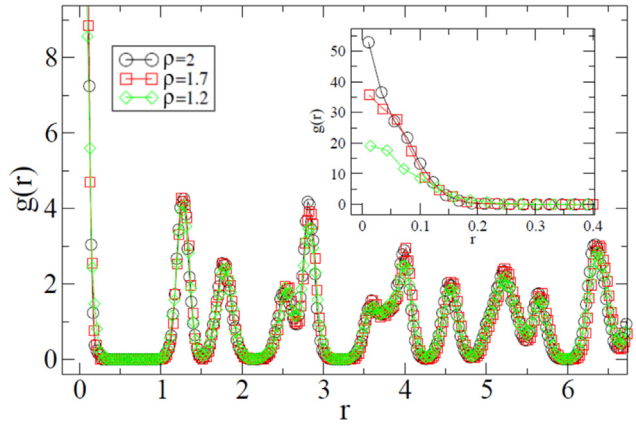

Fig. 17. Radial distribution function. NVT calculations. T = 0.01, N = 1000. ρ = 1.2, 1.7, 2.

5. Conclusions

We showed that many remarkable structures are formed upon self-assembly processes in a model system of particles interacting through a finite repulsion at the origin supplemented by short-range attractive and long-range repulsive competing interactions.

At low and intermediate density we observed quasicrystals with 8-fold, 12-fold and 18-fold crystallographic forbidden symmetries, as well as quasicrystal approximants with local arrangement of particles similar to those characterizing the σ-type and H-type Frank-Kasper phases.

At high densities, due to the finite nature of the repulsion at the origin, particle overlapping becomes relevant, giving origin to peculiar and suggestive patterns. At a surface density approximately equal to one, the system displays a "stripe phase" characterized by the alternance of worm-like parallel stripes of dimers (i.e. two completely or almost completely overlapped particles) and single particles. Upon slightly increasing the density, particles form remarkable clusters consisting in a doubly occupied central site surrounded by two concentric circumferences each of which

is formed by twelve singly occupied equally spaced sites. Such clusters are characterized by a 12-fold symmetry, which sets them apart from the dodecagonal clusters described in the literature on quasicrystals, having an outer dodecagonal contour but possessing just a six-fold symmetry. The clusters observed in our system are mostly arranged according to a square-triangle tiling and their centers form H-type, σ-type and also hexagonal local environments.

At very high densities, particle overlapping becomes dominant and the system forms crystals with multiple occupied sites. Above a given density (around 1.2) the crystal lattice remains unchanged, both as it regards its nature (square geometry) and the value of the reticular constant, while the site occupancy increases with the density, giving origin to trimers, tetramers, etc.

CRediT authorship contribution statement

Gianpietro Malescio: Conceptualization, Methodology, Software, Validation, Formal analysis, Investigation, Resources, Data curation, Writing – original draft, Writing – review & editing, Visualization, Supervision, Project administration, Funding acquisition. **Francesco Sciortino:** Conceptualization, Methodology, Software, Validation, Formal analysis, Investigation, Resources, Data curation, Writing – original draft, Writing – review & editing, Visualization, Supervision, Project administration, Funding acquisition.

Declaration of Competing Interest

The authors declare that they have no known competing financial interests or personal relationships that could have appeared to influence the work reported in this paper.

Acknowledgements

FS acknowledges support from MIUR-PRIN (Grant No. 2017Z55KCW).

References

[1] D. Levine, P.J. Steinhardt, Quasicrystals: a new class of ordered structures, Phys. Rev. Lett. 53 (26) (1984) 2477–2480.
[2] W. Steurer, Twenty years of structure research on quasicrystals. Part I. Pentagonal, octagonal, decagonal and dodecagonal quasicrystals, Z. Kristallogr. 219 (2004) 391–446.
[3] X. Zeng, G. Ungar, Y. Liu, V. Percec, A.E. Dulcey, J.K. Hobbs, Supramolecular dendritic liquid quasicrystals, Nature 428 (6979) (2004) 157–160.
[4] K. Hayashida, T. Dotera, A. Takano, Y. Matsushita, Polymeric quasicrystal: mesoscopic quasicrystalline tiling in ABC starpolymers, Phys. Rev. Lett. 98 (2007) 195502.
[5] S. Fischer, A. Exner, K. Zielske, J. Perlich, S. Deloudi, W. Steurer, P. Lindner, S. Förster, Colloidal quasicrystals with 12-fold and 18-fold diffraction symmetry, Proc. Natl. Acad. Sci. USA 108 (5) (2011) 1810–1814.
[6] C. Xiao, N. Fujita, K. Miyasaka, Y. Sakamoto, O. Terasaki, Dodecagonal tiling in mesoporous silica, Nature 487 (7407) (2012) 349–353.
[7] J. Mikhael, J. Roth, L. Helden, C. Bechinger, Archimedean-like tiling on decagonal quasicrystalline surfaces, Nature 454 (7203) (2008) 501–504.
[8] M.E. Zoorob, M.D.B. Charlton, G.J. Parker, J.J. Baumberg, M.C. Netti, Complete photonic bandgaps in 12-fold symmetric quasicrystals, Nature 404 (6779) (2000) 740–743.
[9] Z.V. Vardeny, A. Nahata, A. Agrawal, Optics of photonic quasicrystals, Nat. Photonics 7 (3) (2013) 177–187.
[10] C. Jin, B. Cheng, B. Man, Z. Li, D. Zhang, S. Ban, B. Sun, Band gap and wave guiding effect in a quasiperiodic photonic crystal, Appl. Phys. Lett. 75 (1999) 1848.
[11] E. Macia, Exploiting aperiodic designs in nanophotonic devices, Rep. Prog. Phys. 75 (2012) 036502.
[12] M. Engel, H.R. Trebin, Self-assembly of monatomic complex crystals and quasicrystals with a double-well interaction potential, Phys. Rev. Lett. 98 (2007) 225505.
[13] T. Dotera, T. Oshiro, P. Ziherl, Mosaic two-length scale quasicrystals, Nature 506 (7487) (2014) 208–211.
[14] H. Pattabhiraman, A.P. Gantapar, M. Dijkstra, On the stability of a quasicrystal and its crystalline approximant in a system of hard disks with a soft corona, J. Chem. Phys. 143 (2015) 164905.
[15] H.G. Schoberth, H. Emmerich, M. Holzinger, M. Dulle, S. Förster, T. Gruhn, Molecular dynamics study of colloidal quasicrystals, Soft Matter 12 (36) (2016) 7644–7654.
[16] A. Reinhardt, F. Romano, J.P.K. Doye, Computing phase diagrams for a quasicrystal-forming patchy-particle system, Phys. Rev. Lett. 110 (2013) 255503.
[17] C.R. Iacovella, A.S. Keys, S.C. Glotzer, Self-assembly of soft-matter quasi crystals and their approximants, Proc. Natl. Acad. Sci. USA 108 (52) (2011) 20935–20940.
[18] A.J. Archer, A.M. Rucklidge, E. Knobloch, Quasicrystalline order and a crystal-liquid state in a soft-core fluid, Phys. Rev. Lett. 111 (2013) 165501.
[19] M. Zu, P. Tan, N. Xu, Forming quasicrystals by monodisperse soft core particles, Nat. Commun. 8 (2017) 2089.
[20] A.A. Louis, P.G. Bolhuis, J.P. Hansen, E.J. Meijer, Can Polymer Coils Be Modeled as "Soft Colloids"?, Phys Rev. Lett. 85 (2000) 2522.
[21] C.N. Likos, M. Schmidt, H. Löwen, M. Ballauff, D. Pötschke, P. Lindner, Soft interaction between dissolved flexible dendrimers: theory and experiment, Macromolecules 34 (2001) 2914–2920.
[22] C.N. Likos, Effective interactions in soft condensed matter physics, Phys. Reports 348 (4-5) (2001) 267–439.
[23] G. Malescio, F. Sciortino, Aggregate formation in fluids with bounded repulsive core and competing interactions, J. Mol. Liquids 303 (2020) 112601.
[24] D. Frenkel, B. Smit, Understanding Molecular Simulation: From Algorithms to Applications, Academic Press, 2002.
[25] F.C. Frank, J.S. Kasper, Complex alloy structures regarded as sphere packings. I. Definitions and basic principles, Acta Crystallogr. 11 (1958) 184.
[26] F.C. Frank, J.S. Kasper, Complex alloy structures regarded as sphere packings. II. Analysis and classification of representative structures, Acta Crystallogr. 12 (1959) 483.
[27] X. Zeng, G. Ungar, Inflation rules of square-triangle tilings: from approximants to dodecagonal liquid quasicrystals, Philos. Mag. 86 (2006) 1093–1103.
[28] M.N. van der Linden, J.P.K. Doye, A.A. Louis, Formation of dodecagonal quasicrystals in two-dimensional systems of patchy particles, J. Chem. Phys. 136 (2012) 054904.
[29] D. Frettlöh, E. Harriss, F. Gähler: Tilings Encyclopedia, https://tilings.math.uni-bielefeld.de.
[30] P. Stampfli, A dodecagonal quasiperiodic lattice in two dimensions, Helv. Phys. Acta 59 (1986) 1260.
[31] C.N. Likos, M. Watzlawek, H. Löwen, Freezing and clustering transitions for penetrable spheres, Phys. Rev. E 58 (3) (1998) 3135–3144.
[32] C.N. Likos, B.M. Mladek, D. Gottwald, G. Kahl, Why do ultrasoft repulsive particles cluster and crystallize? Analytical results from density-functional theory, J. Chem. Phys. 126 (2007) 224502.